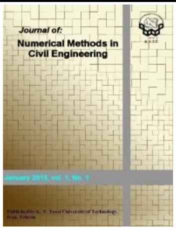


Numerical Methods in Civil Engineering

# The effects of cut-off walls on repulsing saltwater based on modeling of density-driven groundwater flow and salt transport

**Zahra Jamshidzadeh*, Hasan Ghasemzadeh****

*ARTICLE INFO*
*Article history:*
*Received:*
*November 2016.*
*Revised:*
*March 2017.*
*Accepted:*
*April 2017.*

*Keywords:*
*saltwater intrusion; flow and solute transport; density-driven flow; Henry problem; cut-off wall.*

***Abstract:***

*A two-dimensional fully implicit finite difference model, which can be easily extended to three dimensions, is developed to study the effect of cut-off walls on saltwater intrusion into the aquifers. This model consists of a coupled system of two nonlinear partial differential equations which describe unsteady density-driven groundwater flow and solute transport. The numerical model is verified by the Henry problem. A good agreement between this model and the semianalitical solution of Henry problem shows the efficiency of this method for seawater intrusion problems. The effect of cut-off walls on reduction of saltwater intrusion in the Henry problem is investigated. Furthermore, the effect of geometric parameters of the cut-off wall such as depth and distance from the coast on repulsing saltwater is considered. Subsequently, the application of the presented model is considered to evaluate the effect of cut-off wall on repulsing salt water intruded by a pumping well located above the transition zone, which demonstrates that the cut-off wall has strong impact on repulsing saltwater intruded. For example, it repulses more than 45% salt water intruded by the discharge well in the Henry problem.*

## 1. Introduction

Groundwater is the major source of drinking water and agricultural irrigation in many parts of the world. One of the most important problems specifically in the case of coastal aquifers is saltwater intrusion, which is the consequence of over exploitation and the decline of groundwater table. During the past two decades, modeling of saltwater intrusion problems in different parts of the world has been studied by various researchers. These mathematical models have been categorized as sharp interface models and density-driven models. The sharp interface models have been studied by a number of researchers (Paster et al. 2006[27], Ataie-Ashtiani 2007[3], Antonellini et al. 2008 [2], and Shi et al. 2011 [28]) in order to investigate saltwater intrusion problems by simulating freshwater and saltwater as immiscible fluids separated by a sharp interface. However, these models are generally applicable under certain conditions where the width of transition zone is small in comparison with the aquifer thickness.

Investigation of saltwater intrusion based on density-driven models have been performed by some researchers such as: Kolditz et al. 1997[19], Zhang et al. 2004[31], Hughes & Sanford 2004[13], Werner & Gallagher 2006[30], Insigne & Kim 2010[15], Delsman et al. 2014[9]. Kopsiaftis et al. 2009[20] used a finite element model to consider this phenomenon in an unconfined aquifer on Thira Island. Paniconi et al. 2001[26] investigated the occurrence of saltwater intrusion into the Korba coastal plain in Tunisia by using a finite element model called CODESA-3D. Moreover, several codes are available to simulate saltwater intrusion, such as: HST3D (Kipp 1986[18]), SWICHA (Huyakorn et al. 1987[14]), MOCDENSE3D (Oude Essink 1998[25]), FEFLOW (Diersch & Kolditz, 1998[10]), ROCKFLOW (Kolditz et al. 1997[19]), TVDT3D (Ackerer

*Assistant professor, Faculty of Engineering, University of Kashan, Kashan, Iran, , Email: jamshidzadeh@kashanu.ac.ir*

**Corresponding Author: Associate professor, Dept. of Civil Eng., K.N. Toosi University of Technology, Tehran, Iran,,Email: ghasemzadeh@kntu.ac.ir.*

et al. 1999[1]), SUTRA (Voss & Provost, 2002[29]), SEAWAT (Guo & Langevin, 2002[11]). Langevin et al. (2003) [21] used SEAWAT to estimate rate of submarine groundwater discharge to a coastal marine estuary. Lin et al. (2009) [22] used SEAWAT code to investigate saltwater intrusion in Alabama Gulf Coast, USA.

The cut-off walls are widely used in environmental control systems to prevent the lateral spread of liquid or gaseous contaminants. The uses of cut-off walls to prevent saltwater intrusion into the coastal aquifers are common in many parts of the world. This method has been suggested by many researchers to minimize saltwater encroachment (Bear et al. 1999[5]; Luyun et al. 2008[23]; Bear & Cheng 2010[6]; Kaleris & Ziogas 2013[17]). For example, there are about 15 subsurface dams in Japan, seven of which have been constructed into the coastal aquifers to prevent saltwater intrusion (Luyun et al. 2009[24]). Luyun et al. (2009)[24] studied laboratory-scale of cutoff walls to investigate the effect of cut off wall depth on saltwater repulsing. Their study revealed that a shorter cutoff wall achieved a faster removal rate of saltwater than a higher wall. Crestani et al. (2017)[7] studied a numerical and physical modeling of cutoff walls against saltwater intrusion in a homogenous coastal aquifer by using the SUTRA code. The results of their study showed that the cutoff wall is effective in reducing the vertical extent of the salt wedge even if a large amount of incoming freshwater is extracted from the draining trench.

In this study, a fully implicit finite difference code is developed to simulate coupled density-driven flow and transport in anisotropic and non-homogenous porous media. The Picard iteration method is used for the numerical solution of the nonlinear coupled system of governing equations. To verify the numerical code, the Henry problem [12] which is the famous density-driven fluid flow and salt transport benchmark is examined. It provides a well-defined semi-analytical solution of seawater intrusion into a confined aquifer. The aim of this study is to assess the effectiveness of cut-off walls on repulsing seawater intrusion for different cut-off wall geometric parameters such as depth and distance from the coast. All investigations are performed by using a numerical code and are tested in the Henry problem. Also, the application of the presented model is considered to evaluate the effect of cut-off wall on repulsing salt water intruded by a pumping well located above the transition zone.

## 2. Mathematical Model

In order to simulate coupled groundwater flow and salt transport in porous media, the following governing equations, based on the mass conservation laws, Darcy's law, and Fick's law are employed.

### *2.1. Governing Equations*

#### *2.1.1. Flow equation*

Based on the mass conservation law, the density-driven flow equation is (Bear 1979 [4])

$$\frac{\partial(\rho\theta)}{\partial t}+\nabla.\left(\rho\mathbf{q}+\theta\mathbf{J}^{*\rho}\right)=0 \tag{1}$$

where $\rho$ is water density [$ML^{-3}$], $\mathbf{q}$ is the Darcy velocity [$MT^{-1}$], $\mathbf{J}^{*\rho}$ is the dispersive flux of total fluid mass [$ML^{-2}T^{-1}$] and, $t$ is time [T]. The Darcy velocity of density-driven flow in terms of freshwater head is (Bear 1979[4])

$$\mathbf{q}=-\frac{\mathbf{k}\rho_f\, g}{\mu}\left[\nabla h_f+\left(\frac{\rho-\rho_f}{\rho_f}\right)\nabla z\right] \tag{2}$$

where $\mathbf{k}$ is the intrinsic permeability tensor [$L^2$], $\mu$ is the dynamic viscosity [$ML^{-1}T^{-1}$], $\rho_f$ is the reference freshwater density [$ML^{-3}$], $h_f$ is freshwater head [L], $g$ is the gravitational acceleration [$LT^{-2}$], and $z$ is the elevation [L].

Discarding the effect of temperature, the fluid density and dynamic viscosity are functions of salt concentration. So, the equation of state for fluid density considered by (Bear 1979 [4]) is,

$$\rho(C)=\rho_f\left[1+\beta C\right] \tag{3}$$

where $\rho_f$ is freshwater density, C [$ML^{-3}$] is salt concentration, and $\beta$ is the salt concentration coefficient [$M^{-1}L^3$].

The salt concentration coefficient can be approximated by (Bear 1979[4])

$$\beta=\frac{1}{\rho_f}\frac{\partial\rho}{\partial C}\approx\frac{1}{\rho_f}\left(\frac{\rho_{\max}-\rho_f}{C_{\max}}\right) \tag{4}$$

where $\rho_{\max}$ [$ML^{-3}$] is the maximum density of water, and $C_{\max}$ [$ML^{-3}$] is the maximum concentration of salt.

The dynamic viscosity is a nonlinear function of salt concentration and density, which can be expressed as (Bear & Cheng 2010[6])

$$\mu(C)=\mu_{f0}\left[1+1.85\left(\frac{C}{\rho}\right)-4.1\left(\frac{C}{\rho}\right)^2+44.5\left(\frac{C}{\rho}\right)^3\right] \tag{5}$$

where $\mu_{f0}$ is the dynamic viscosity, corresponds to C=0.

#### *2.1.2. Salt transport equation*

In the absence of source/sink term, the advection-dispersion equation of salt transport can be described by (Bear 1979[4])

$$\frac{\partial(\theta C)}{\partial t}-\nabla.\left(\theta\mathbf{D}_h\nabla C\right)+\nabla.\left(\mathbf{q}C\right)=0 \tag{6}$$

The hydrodynamic dispersion tensor is expressed by Scheidegger's formula as follows (Bear 1979[4]):

$$\mathbf{D}_{ijh}=\alpha_T\left|\mathbf{v}\right|\delta_{ij}+\left(\alpha_L-\alpha_T\right)\frac{\mathrm{v}_i\mathrm{v}_j}{\left|\mathbf{v}\right|}+\boldsymbol{\tau}D_m \tag{7}$$

where $\mathbf{D}_{ijh}$ is the hydrodynamic dispersion tensor, $\alpha_L$ and $\alpha_T$ are the longitudinal dispersivity and transverse dispersivity [L], respectively, $D_m$ is the molecular diffusion coefficient [$L^2T^{-1}$], $\mathbf{v}$ is the seepage velocity [$LT^{-1}$], which is $\mathbf{v}=\mathbf{q}/\theta$ , $|\mathbf{v}|$ is the magnitude of the seepage velocity, $\delta_{ij}$ is the Kronecker delta, and $\boldsymbol{\tau}$ is a second rank symmetric tensor, representing the tortuosity of the porous medium which for isotropic saturated porous media may be represented as $\boldsymbol{\tau}=\tau\delta_{ij}$ in which, $\tau$ is a scalar tortuosity equal to $\tau=\theta^{\frac{1}{3}}$ for saturated porous media (Bear & Cheng 2010[6]). The first two terms on the right side of equation (7) represent the mechanical dispersion term. The third term represents the effective diffusion term, which depends on both the molecular diffusion of brine in water and the porous medium tortuosity.

*2.2. Numerical solutions for density-driven flow and transport*

The system of the coupled governing equations (1) and (6) is nonlinear. In this study, we simulate density-driven flow and transport in two-dimensional cross sections. According to equation (1), the extended form of density-driven saturated flow equation in terms of freshwater head is

$$\frac{\rho}{\rho_f}S_f\frac{\partial h_f}{\partial t}+\theta\beta\frac{\partial C}{\partial t}= \frac{\partial}{\partial x}\left\{\left(\frac{k_x\rho g}{\mu}\frac{\partial h_f}{\partial x}\right)\right\}+\frac{\partial}{\partial z}\left\{\left[\frac{k_z\rho g}{\mu}\left(\frac{\partial h_f}{\partial z}+\frac{\rho-\rho_f}{\rho_f}\right)\right]\right\} \tag{8}$$

where $S_f$ is the specific storage in terms of freshwater head [$L^{-1}$]. It must be notice that the flow equation is based on the assumption that the principal directions of the intrinsic permeability in anisotropic porous media are aligned with the selected coordinate system, i.e. in x and z directions. So, $k_{xz}=k_{zx}=0$.

The extended form of non-reactive salt transport equation, neglecting any source/sink is

$$\frac{\partial(\theta C)}{\partial t}= \frac{\partial}{\partial x}\left\{\theta D_{xx}\frac{\partial C}{\partial x}+\theta D_{xz}\frac{\partial C}{\partial z}\right\}+\frac{\partial}{\partial z}\left\{\theta D_{zz}\frac{\partial C}{\partial z}+\theta D_{zx}\frac{\partial C}{\partial x}\right\} +\frac{\partial}{\partial x}\left(\frac{k_x\rho_f g}{\mu}C\frac{\partial h_f}{\partial x}\right)+\frac{\partial}{\partial z}\left\{\frac{k_z\rho_f g}{\mu}C\left(\frac{\partial h_f}{\partial z}+\frac{\rho-\rho_f}{\rho_f}\right)\right\} \tag{9}$$

Using the block-centered finite difference discretization scheme in the flow equation, and the Picard iteration scheme for the nonlinear terms, the fully implicit approximate of the two-dimensional density driven of flow equation is:

$$A_1 h_{f\,i-1,j}^{\,n+1,m+1}+B_1 h_{f\,i,j}^{\,n+1,m+1}+C_1 h_{f\,i+1,j}^{\,n+1,m+1}+D_1 h_{f\,i,j-1}^{\,n+1,m+1} +E_1 h_{f\,i,j+1}^{\,n+1,m+1}=F_1 h_{f\,i,j}^{\,n}+RHS(C)^{n+1,m} \tag{10}$$

where $A_1$ to $F_1$ are the numerical coefficients as a function of fluid properties and solid permeability between two nodes which have been calculated based on harmonic mean, $n$ is the time step, and $m$ is the iteration stage in one time step. *RHS(C)* is the coefficient that depends on salt concentration in previous iteration stage. This term is related to $\mathbf{J}^{*\rho}$ and the hydrodynamic dispersion coefficients. The details in the numerical coefficients are shown in appendix A.

Using the similar scheme, the fully implicit approximate of the two-dimensional salt transport equation is

$$A_2C_{i-1,j}^{\,n+1,m+1}+B_2C_{i,j}^{\,n+1,m+1}+C_2C_{i+1,j}^{\,n+1,m+1}+D_2C_{i,j-1}^{\,n+1,m+1}+E_2C_{i,j+1}^{\,n+1,m+1} +F_2C_{i+1,j+1}^{\,n+1,m+1}+G_2C_{i-1,j+1}^{\,n+1,m+1}+H_2C_{i+1,j-1}^{\,n+1,m+1}+I_2C_{i-1,j-1}^{\,n+1,m+1}=J_2C_{i,j}^{\,n} \tag{11}$$

where $A_2$ to $J_2$ are the numerical coefficients which are shown in appendix A.

The linearized system of equations (10) and (11) are solved using the Gaussian Elimination method. At the end of each iteration stage, the fluid density, the fluid viscosity, and the Darcy velocities are updated by the following equations:

$$\rho_{i,j}^{n+1,m+1}=\rho_f\left[1+\beta\left(C_{i,j}^{\,n+1,m+1}\right)\right] \tag{12}$$

$$\mu_{i,j}^{n+1,m+1}=\left[1+1.85\left(\frac{C_{i,j}^{\,n+1,m+1}}{\rho_{i,j}^{n+1,m+1}}\right)-4.1\left(\frac{C_{i,j}^{\,n+1,m+1}}{\rho_{i,j}^{n+1,m+1}}\right)^2+44.5\left(\frac{C_{i,j}^{\,n+1,m+1}}{\rho_{i,j}^{n+1,m+1}}\right)^3\right] \tag{13}$$

$$q_{x_{i,j}}^{\,n+1,m+1}=-\frac{k_x\rho_f g}{\mu_{i,j}^{n+1,m+1}}\left(\frac{h_{f\,i+1,j}^{\,n+1,m+1}-h_{f\,i-1,j}^{\,n+1,m+1}}{2\Delta x}\right) \tag{14}$$

$$q_{z_{i,j}}^{\,n+1,m+1}=-\frac{k_z\rho_f g}{\mu_{i,j}^{n+1,m+1}}\left(\frac{h_{f\,i,j+1}^{\,n+1,m+1}-h_{f\,i,j-1}^{\,n+1,m+1}}{2\Delta z}+\frac{\rho_{i,j}^{n+1,m+1}-\rho_f}{\rho_f}\right) \tag{15}$$

The Picard iteration method is used to obtain the numerical solutions of the nonlinear coupled equations. The solution procedure is as follows. In the first time step, the freshwater head is calculated by equation (10), where the numerical coefficients and $RHS(C)$ are calculated based on the initial conditions. Then, the Darcy velocities are calculated by the initial fluid density and viscosity and the new freshwater head. The salt concentration is calculated by equation (11), where numerical coefficients are calculated with the initial fluid density and viscosity and the new Darcy's velocities. The calculated salt concentration is used to update the fluid density and viscosity. The freshwater head and salt concentration are re-calculated by solving equations (10) and (11) using the updated fluid density and viscosity. The iteration procedure is repeated until the following convergence criteria is met:

$$\left|h_f^{\,n+1,m+1}-h_f^{\,n+1,m}\right|\le\delta_h=10^{-2} \tag{16}$$

$$\left|C^{n+1,m+1} - C^{n+1,m}\right| \le \delta_c = 10^{-2} \quad (17)$$

Subsequently, the calculations move to the next time step.

## 3. Numerical Results and Discussion

### *3.1. Code Verification (Henry Problem)*

Using benchmark problems to verify any numerical code is one of the most important steps to test the correctness of the numerical approximations. The Henry problem has been discussed extensively in the literature as a seawater intrusion benchmark for moderate density-driven groundwater flow in an isotropic and homogenous confined aquifer. The problem is a diffusive flow with an exaggerated molecular diffusion coefficient, while the mechanical dispersion is neglected ($\alpha_L=\alpha_T=0$) (Henry 1964[12]). The spatial dimension and boundary conditions of the Henry problem are shown in Figure 1. The top and bottom boundaries are impervious. The flow domain initially is full of freshwater. The initial hydraulic head is set to unity. Table 1 lists the model parameters of the Henry problem. In this part, the numerical code is tested based on the traditional sea boundary condition. A grid size of 21 rows and 41 columns is used to discretize the domain which corresponds to a uniform discretization with $\Delta x=\Delta z=0.05$ m, and with the time step at 6 seconds, the steady-state solution is obtained after 300 minutes. Simulation after 300 minutes shows no significant changes in the results. The simulated steady-state positions of isochlors shown in Figure 2(a) are compared well to the semi-analytical solution and the previous published numerical solutions. Figure 2(b) shows the freshwater head distribution and the flow field [16].

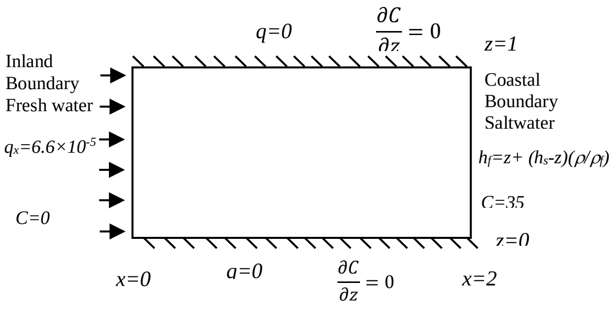


**Fig.1:** Domain and boundary conditions for the Henry's problem

**Table.1**: The Henry's problem parameters [12]

| Parameter | Symbol | Value | Unit |
|---|---|---|---|
| Hydraulic Conductivity | $K$ | $1.0\times10^{-2}$ | $ms^{-1}$ |
| Molecular diffusion coefficient | $D_m$ | $1.886\times10^{-5}$ | $m^2s^{-1}$ |
| Recharge inflow | $Q$ | $6.\ 6\times10^{-5}$ | $ms^{-1}$ |
| Specific storage | $S_f$ | 0.00 | $m^{-1}$ |
| Porosity | $\theta$ | 0.35 | --- |
| Longitudinal dispersivity | $\alpha_L$ | 0.01 | M |
| Longitudinal dispersivity | $\alpha_T$ | 0.01 | M |
| Freshwater Density | $\rho_f$ | 1000 | kg $m^{-3}$ |
| Saltwater Density | $\rho_{max}$ | 1025 | kg $m^{-3}$ |
| Saltwater concentration | $C_{max}$ | 35 | kg $m^{-3}$ |
| Freshwater concentration | $C_f$ | 0 | kg $m^{-3}$ |

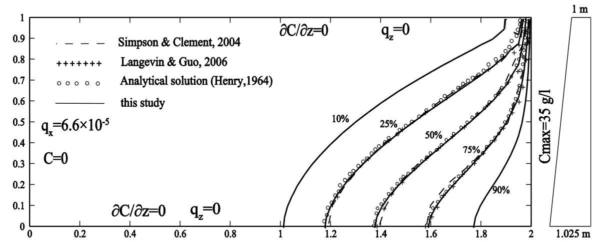


**Fig.2:** 10%, 25%, 50%, 75% and 90% isochlor curves of the Henry problem (after 300 minutes) [16].

### *3. 2. The effect of cut-off wall on control of saltwater intrusion*

In this part, the effect of cut-off wall on the Henry problem saltwater intrusion is examined to evaluate the location of isochlor curves and the head distribution. All simulation parameters are similar to the Henry problem. Hydraulic conductivity and porosity of the cut-off wall are assumed equal to $7.23\times10^{-9}$ m/s and 0.4 (Daniel and Koerner 2000[8]), respectively. The cut-off wall thickness is assumed equal to 10 cm. Three different cases are considered here which are shown in figure 3(a)-(c). Figures (4)-(6) exhibit the simulation results for salt distribution, head distribution and velocity field at the end of the analysis for each case. It is observed that the invading of saltwater in case (1) is less than case (2) which is reasonable.

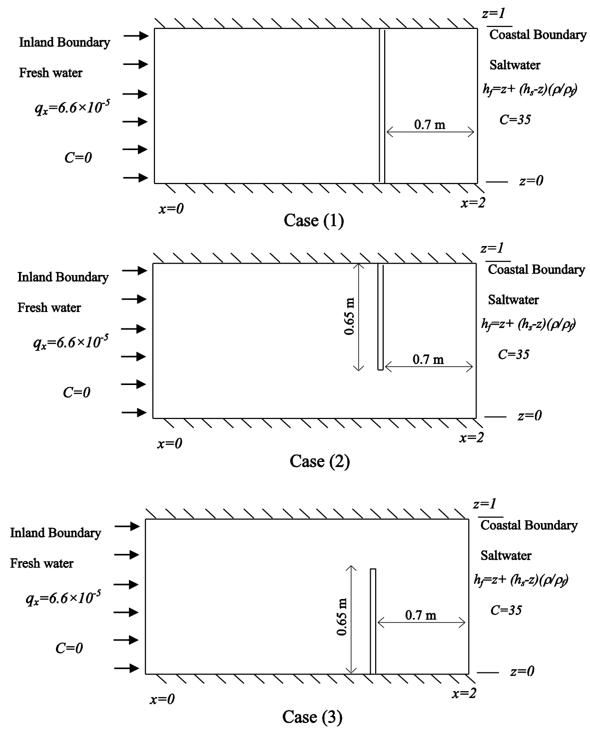


**Fig. 3:** The location of cut-off wall in the Henry problem for different cases

For case (3), the cut-off wall has no considerable effect in preventing saltwater intrusion which may be due to the unsuitable position of the cut-off wall and seaward boundary condition. As expected, the velocity vectors far from the cut-off wall are horizontal, while they are vertical near the cut-off wall. The small permeability of the cut-off wall material prevents the flow of fluid through it and therefore, the fluid path is changed and fluid vectors become vertical close to the cut-off wall.

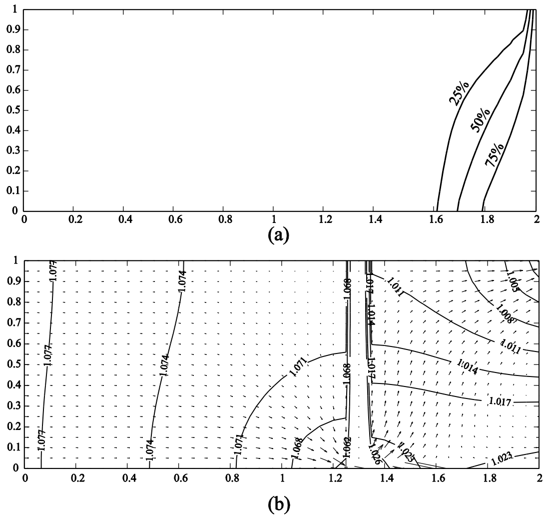


**Fig. 4:** The effect of vertical cut-off wall on Henry problem for Case (1): (a) 25%, 50% and 75% isochlor curves and (b) freshwater head distribution and flow field (after 300 minutes).

Figure (7) shows position of the 50% isochlor curve for different depths of the cut-off wall. It is observed that increasing the cut-off wall depth generates the best result for salt water intrusion control when a cutoff wall is located in an area of saltwater intrusion. Figure (8) shows the changes in the position of the 25%, 50%, and 75% isochlor curve versus the changes in cut-off wall distance from the coast. The cut-off wall depth is 0.75 m and the other parameters are the same as before. These numerical simulations have shown that the optimum location for the cut-off wall is near the seaward boundary and by moving away from the seaward boundary, the rate of salt water intrusion increases. It should be stated that these results can only be used for problems possessing the same initial and boundary conditions.

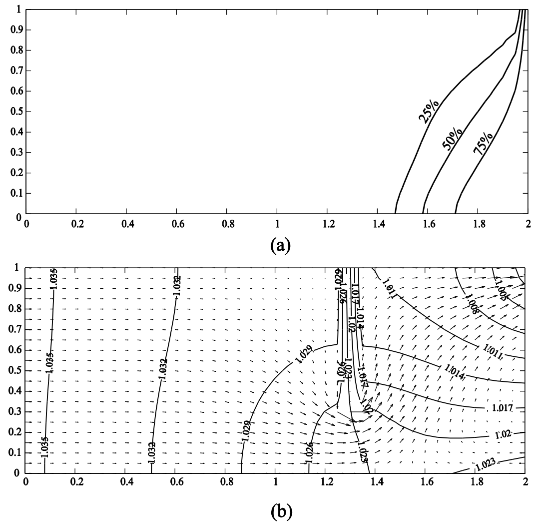


**Fig. 5:** The effect of vertical cut-off wall on Henry problem for Case (2): (a) 25%, 50% and 75% isochlor curves and (b) freshwater head distribution and flow field (after 300 minutes).

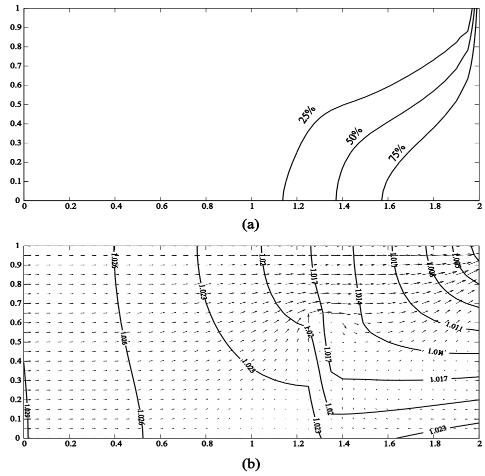


**Fig. 6:** The effect of vertical cut-off wall on Henry problem for Case (3): (a) 25%, 50% and 75% isochlor curves and (b) freshwater head distribution and flow field (after 300 minutes).

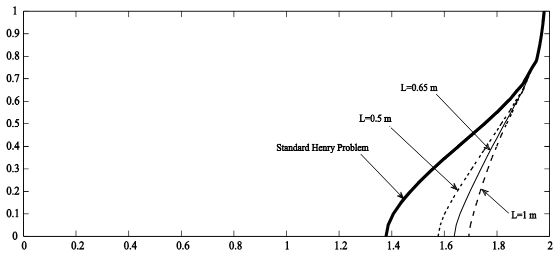


**Fig.7:** Position of the 50% isochlor curve in the aquifer for different cut-off wall depth in Henry problem (after 300 minutes).

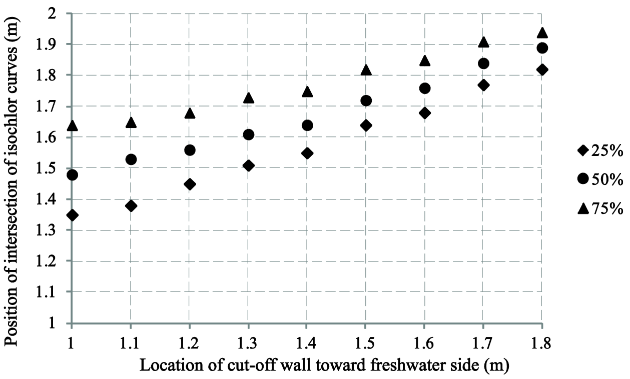


**Fig. 8:** Position of the isochlor curves intersection with the base of the aquifer versus the change in location of cut-off wall

A quantitative indicator to characterize the effectiveness of the cut-off walls is the percentage reduction of total salt which is defined as:Figure (9) shows the changes in total salt reduction versus changes in the cut-off wall distance from the coast. Assuming the depth of the cut-off wall to be 0.75 m and maintaining the other parameters the same as before, it is observed that in this case, the best location for the cut-off wall is at 0.3 m distance from the coast. Getting closer than 0.3 m to the seaward could have unpredictable consequences which may be caused due to the existence of a circulation flow in the lower part of the seaward. By getting away from the coast, the effect of cut-off becomes insignificant. It is the emphases of this fact that the cut-off wall can effectively reduce saltwater intrusion if they are constructed in the area of the saltwater wedge (Luyun et al. 2008[23]). The effect of cut-off wall depth on the percentage reduction of total salt is presented in Figure (10). It shows the percentage reduction of total salt versus changes in the cut-off wall depth which is located at 0.7 m from the coast. It can be noticed that increasing the cut-off wall depth leads to growth in the percentage reduction of total salt which is reasonable.

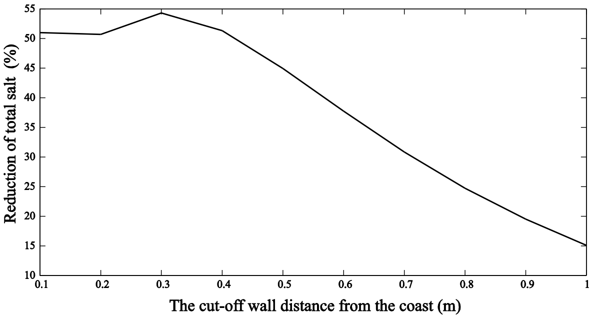


**Fig. 9:** The percentage reduction of total salt versus cut-off wall distance from the coast

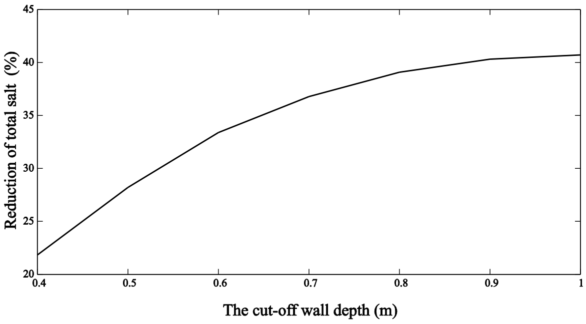


**Fig. 10:** The percentage reduction of total salt versus cut-off wall depth

*3.3. The effect of cut-off wall to repulsing of saltwater intruded by the discharge well*

In this section, the presented method is used to consider the effect of cut-off wall on repulsing saltwater intruded by a discharge well. Two cases are studied here.

*3.3.1. Case A- Seawater intrusion into the aquifer by a* discharge *well*

To consider the effect of discharge wells on saltwater encroachment into the aquifer, a discharge well was located at x=1.5 m and z=0.85 m in the Henry problem. It is assumed that the discharge well pumps out about $1\times10^{-5}$ $m^3/s$ of the total recharge inflow. In this case, the results obtained from the steady-state solution of standard Henry problem have been used as the initial conditions for this simulation and the model was operated to achieve a steady-state condition.

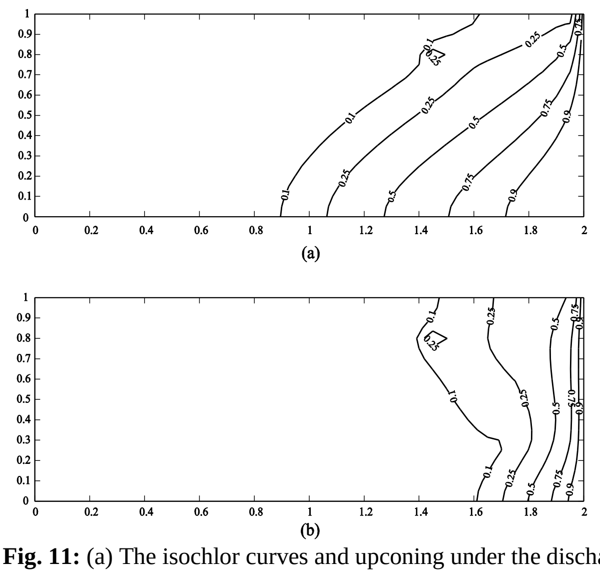


**Fig. 11:** (a) The isochlor curves and upconing under the discharge well after 200 minutes and (b) the isochlor curves after putting the cut-off wall after 180 minutes simulation time

Figure (11-a) shows the salt concentration profiles for this case after 200 minutes simulation times to reach a new steady-state condition. It is observed that the upconing phenomenon takes place under the well and the low isochlor curves are more sensitive to upconing than higher isochlor curves. Also, the discharge well leads to more saltwater encroachment into the aquifer. In this case, after 200 minutes, about 40% of aquifer volume is occupied by saltwater and reaches a steady-state condition.

*3.3.3. Case B- The effect of the cut-off wall on repulsing salt water intrusion.*

In this case, a cut-off wall was located at *x=1.75 m* from the coast in the Henry problem. In this section, the results obtained from the steady-state solution of Case (A) are used as the initial conditions for this simulation to consider the effect of the cut-off wall on repulsing salt water intruded by the discharge well. Figure (11-b) shows the salt concentration profiles for this case after 180 minutes simulation times. Longer simulation shows no significant changes in solution. It observed that the cut-off wall repulsed about 45% of salt water intruded into the aquifer. It is noticed that during the simulation of this case, the discharge well has pumped the water and the decay of the salt water up-coning to the well by shutting off the discharge well, has not been considered.

## 4. Conclusions

The main objective of this study was to show the importance of the cut-off walls in groundwater management and to control and repulse of saltwater intrusion into the aquifer. A numerical modeling of saltwater intrusion based on density-driven groundwater flow was presented using a fully implicit finite difference method to solve the coupled flow and salt concentration governing equations in non-homogeneous anisotropic porous media. The Picard iteration method is used to handle the nonlinearity in the coupled system and to obtain numerical solutions. In order to verify the presented model, the Henry problem 1964 [12] as a standard benchmark for saltwater intrusion was examined and results of salt concentration were compared with the results of other researchers. A good agreement between the presented method and previously published solutions from other researchers shows the efficiency of this code for seawater intrusion problems. Also, the effect of cut-off walls on prevention of saltwater encroachment into the aquifer were considered. The amount of salt water intruded depends on the depth and the distance of cut-off walls from the seaward. The results show that any increase in the cut-off wall depth leads to growth in the percentage reduction of total salt which is reasonable. Also, the cut-off wall distance from the coast is very crucial and the cut-off wall can effectively reduce saltwater intrusion if they are constructed in the area of the saltwater wedge. Exploitation of groundwater through the discharge wells lead to saltwater intrusion into coastal aquifers and create up-coning phenomenon under the well discharge. The numerical results showed that in the Henry problem, the cut-off wall could repulse about 45% of salt water intruded by the discharge well into the aquifer. In conclusion, the cut-off walls play an important role in controlling and repulsing salt water intrusion in the coastal aquifer and can be used in groundwater management to prevent water contamination through salinity.

## References


**[1]** Ackerer, Ph., Younès, A., Mosé, R., "Modeling variable density flow and solute transport in porous medium: Numerical model and verification", Transport in porous media, vol. 35, 1999, p.345-373.

**[2]** Antonellini, M., Mollema, P., Giambastiani, B., Bishop, K., Caruso, L., Minchio, A., Pellegrini, L., Sabia, M., Ulazzi, E., Gabbianelli, G, "Salt water intrusion in the coastal aquifer of the southern Po Plain, Italy", Hydrogeology Journal, vol.16, 2008, p.1541–1556.

**[3]** Ataie-Ashtiani, B., "MODSharp: Regional-scale numerical model for quantifying groundwater flux and contaminant discharge into the coastal zone", Journal of Environmental Modeling & Software, vol. 22, 2007, p. 1307-1315.

**[4]** Bear, J., "Hydraulic of groundwater", McGraw-Hill, New York; 1979.

**[5]** Bear, J., Cheng, A.H.D, Sorek, S., Ouazar, D., Herrera, I., "Seawater intrusion in coastal aquifers: concepts, methods and practices, Theory and Applications of Transport in Porous Media", 14.Kluwer, Dordrecht, The Netherlands, 1999.

**[6]** Bear. J., Cheng, A.H.D., "Modeling Groundwater Flow and Contaminant Transport", Springer Dordrecht Heidelberg London, New York 2010, pp 834.

**[7]** Crestani, E., Camporese, M., Salandin, P., "Numerical and physical modeling of cutoff walls against saltwater intrusion", $19^{th}$ EGU General Assembly, EGU 2017, Vienna, Austria, p.18080.

**[8]** Daniel, D.E., Koerner, R.M., "On the use of geomembranes in vertical barriers: Advances in transportation and geoenvironmental systems using geosynthetics", ASCE GSP, vol. 103, 81-93, doi:10.1061/40515(291)5.

**[9]** Delsman, J.R., Hu-a-ng, K.R.M., Vos, P.C., de Louw, P.G.B., Oude Essink, G.H.P., Stuyfzand, P.J., Bierkens, M.F.P., "Paleo-modeling of coastal saltwater intrusion during the Holocene: an application to the Netherlands", Hydrology and Earth System Sciences, vol. 18, 2014, p.3891-3905,

**[10]** Diersch, H.J.G., Kolditz, O., "Coupled groundwater flow and transport: Thermohaline and 3D convection systems", Advances in Water Resources, vol. 21, 1998, p. 401-425.

**[11]** Guo, W., Langevin, C.D., "User's Guide to SEAWAT: A Computer Program for Simulation of Three- Dimensional Variable-Density Ground-Water Flow", Techniques of Water-Resources Investigations of the U.S. Geological Survey; 2002.

**[12]** Henry, H.R., "Effects of dispersion on salt encroachment in coastal aquifers, in Sea Water in Coastal Aquifers", U.S. Geological Survey, vol. 1613-C, 1964, p.70-84.

**[13]** Hughes, J.D., Sanford, W.E., "SUTRA-MS: A Version of SUTRA Modified to Simulate Heat and Multiple-Solute Transport", U.S. Department of the Interior, Geological Survey 2004, p 152.

**[14]** Huyakorn, P.S, Andersen, P.F., Mercer, J.W., White, H.O., "Saltwater intrusion in aquifers-development and testing of a three-dimensional finite-element model", Water Resources Research, vol. 23, 1987, p. 293-312.

**[15]** Insigne, M.L., Kim, G., "Saltwater Intrusion Modeling in the Aquifer Bounded by Manila bay and Paranaque River, Philippines", Environmental Engineering Research, vol. 15(2), 2010, p.117-121.

**[16]** Jamshidzadeh, Z., Tsai, F.T.C., Mirbagheri, S.A., Ghasemazadeh, H., "Fluid dispersion effects on density-driven thermohaline flow and transport in porous media", Advances in Water Resources, vol. 61, 2013, p.12–28.

**[17]** Kaleris, V.K., Ziogas, A.L., "The effect of cutoff walls on saltwater intrusion and groundwater extraction in coastal aquifers", Journal of Hydrology, vol. 476, 2013, p. 370-383.

**[18]** Kipp, K.L.Jr., "Guide to the revised heat and solute transport simulator: HST3D - Version 2", Water-Resources Investigations Report 97-4157, Denver, Colorado. USGS; 1997.

**[19]** Kolditz, O., Ratke, R., Diersch, H.J.G., Zielke, W., "Coupled groundwater slow and transport: 1. Verification of variable density flow and transport models", Advances in Water Resources, vol. 21, 1997, p. 27-46.

**[20]** Kopsiaftis, G., Mantoglou, A., Giannoulopoulos, P., "Variable density coastal aquifer models with application to an aquifer on Thira Island", Journal of Desalination, vol. 237, 2009, p.65-80.

**[21]** Langevin, C.D., Shoemaker, W. B., Guo, W., "MODFLOW-2000, the U.S. Geological Survey Modular Ground-Water Model-Documentation of the SEAWAT-2000 Version with the Variable-Density Flow Process (VDF) and the Integrated MT3DMS Transport Process (IMT)", U.S. Geological Survey, Miami 2003; p 54.

**[22]** Lin, J., Snodsmith, J.B., Zheng, Ch., Wu, J., "A modeling study of seawater intrusion in Alabama Gulf Coast, USA", Journal of Environmental Geology, vol. 57, 2009, p.119-130.

**[23]** Luyun, R. Jr., Momii, K., Nakagawa, K., Fujiyama, S., "Saltwater dynamics due to cut-off wall installation in coastal unconfined aquifers: experimental and numerical studies, Calibration and Reliability in Groundwater Modelling: Credibility in Modelling", IAHS Publ., vol. 320, 2008, p. 214-219.

**[24]** Luyun, R., Momii, K., Nakagava, K., Takahashi, M., "Effects of Artificial Reacharge and Physical Barrier on Seawater Intrusion", Annual Journal of Hydraulic Engineering, JSCE, vol. 53, 2009, p. 85-90.

**[25]** Oude Essink, G.H.P., "MOC3D adapted to simulate 3D density-dependent groundwater flow", In Proceedings of MODFLOW '98 Conference at the International Ground Water Modeling Center, Golden, Colorado: Colorado School of Mines, vol. 1, 1998, p. 291-300.

**[26]** Paniconi, C., Khlaifi, I., Lecca, G., Giacomelli, A., Tarhouni, J., "A Modeling Study of Seawater Intrusion in the Korba Coastal Plain, Tunisia", Journal of Physics and Chemistry of Earth (B), vol. 26(4), 2001, p. 345-351.

**[27]** Paster, A., Dagan, G., Guttman, J., "The salt-water body in the Northern part of Yarkon-Taninim aquifer: Field data analysis, conceptual model and prediction", Journal of Hydrology, vol. 323, 2006, p. 154–167.

**[28]** Shi, L., Cui, L., Park, N., Huyakorn, P.S., "Applicability of a sharp-interface model for estimating steady-state salinity at pumping wells—validation against sand tank experiments", Journal of Contaminant Hydrology, vol. 124, 2011, p. 35-42. doi: 10.1016.

**[29]** Voss, C.I., Provost, A.M., "SUTRA- A model for saturated–unsaturated variable-density ground-water flow with solute or energy transport", US Geological Survey Water-Resources Investigations, Report, 02-4231, 2002, p 250.

**[30]** Werner, A.D., Gallagher, M.R., "Characterization of sea-water intrusion in the Pioneer Valley, Australia using hydrochemistry and three-dimensional numerical modeling", Journal of Hydrogeology, vol. 14, 2006, p.1452-1469.

**[31]** Zhang, Q., Volker, R.E., Lockington, D.A., "Numerical investigation of seawater intrusion at Gooburrum, Bundaberg, Queensland, Australia", Journal of Hydrogeology, vol. 12, 2004, p. 674-687.

## Appendix A

The numerical coefficients of flow equation are:

$$A_1 = \frac{2g}{\Delta x^2}\left(\frac{(\frac{k_x\rho}{\mu})^{n+1,m}_{i,j}.(\frac{k_x\rho}{\mu})^{n+1,m}_{i-1,j}}{(\frac{k_x\rho}{\mu})^{n+1,m}_{i,j}+(\frac{k_x\rho}{\mu})^{n+1,m}_{i-1,j}}\right) \quad \text{(A-1)}$$

$$B_1 = -\frac{2g}{\Delta x^2}\left(\frac{(\frac{k_x\rho}{\mu})^{n+1,m}_{i,j}.(\frac{k_x\rho}{\mu})^{n+1,m}_{i+1,j}}{(\frac{k_x\rho}{\mu})^{n+1,m}_{i,j}+(\frac{k_x\rho}{\mu})^{n+1,m}_{i+1,j}}\right) -\frac{2g}{\Delta x^2}\left(\frac{(\frac{k_x\rho}{\mu})^{n+1,m}_{i,j}.(\frac{k_x\rho}{\mu})^{n+1,m}_{i-1,j}}{(\frac{k_x\rho}{\mu})^{n+1,m}_{i,j}+(\frac{k_x\rho}{\mu})^{n+1,m}_{i-1,j}}\right) -\frac{2g}{\Delta z^2}\left(\frac{(\frac{k_z\rho}{\mu})^{n+1,m}_{i,j}.(\frac{k_z\rho}{\mu})^{n+1,m}_{i,j+1}}{(\frac{k_z\rho}{\mu})^{n+1,m}_{i,j}+(\frac{k_z\rho}{\mu})^{n+1,m}_{i,j+1}}\right) -\frac{2g}{\Delta z^2}\left(\frac{(\frac{k_z\rho}{\mu})^{n+1,m}_{i,j}.(\frac{k_z\rho}{\mu})^{n+1,m}_{i,j-1}}{(\frac{k_z\rho}{\mu})^{n+1,m}_{i,j}+(\frac{k_z\rho}{\mu})^{n+1,m}_{i,j-1}}\right)-\frac{\rho^{n+1,m}_{i,j}gS_P}{\Delta t} \quad \text{(A-2)}$$

$$C_1 = \frac{2g}{\Delta x^2}\left(\frac{(\frac{k_x\rho}{\mu})^{n+1,m}_{i,j}.(\frac{k_x\rho}{\mu})^{n+1,m}_{i+1,j}}{(\frac{k_x\rho}{\mu})^{n+1,m}_{i,j}+(\frac{k_x\rho}{\mu})^{n+1,m}_{i+1,j}}\right) \quad \text{(A-3)}$$

$$D_1 = \frac{2g}{\Delta z^2}\left(\frac{(\frac{k_z\rho}{\mu})^{n+1,m}_{i,j}.(\frac{k_z\rho}{\mu})^{n+1,m}_{i,j-1}}{(\frac{k_z\rho}{\mu})^{n+1,m}_{i,j}+(\frac{k_z\rho}{\mu})^{n+1,m}_{i,j-1}}\right) \quad \text{(A-4)}$$

$$E_1 = \frac{2g}{\Delta z^2}\left(\frac{(\frac{k_z\rho}{\mu})^{n+1,m}_{i,j}.(\frac{k_z\rho}{\mu})^{n+1,m}_{i,j+1}}{(\frac{k_z\rho}{\mu})^{n+1,m}_{i,j}+(\frac{k_z\rho}{\mu})^{n+1,m}_{i,j+1}}\right) \quad \text{(A-5)}$$

$$F_1 = -\frac{\rho^{n+1,m}_{i,j}gS_P}{\Delta t} \quad \text{(A-6)}$$

The numerical coefficients of salt equation are:

$$A_2 = a_2 - h_2 - i_2 - j_2 \quad \text{(A-7)}$$

$$B_2 = a_2 + b_2 + c_2 + d_2 + h_2 - g_2 - m_2 - n_2 - o_2 - \frac{\theta}{\Delta t} \quad \text{(A-8)}$$

$$C_2 = b_2 + g_2 + i_2 + j_2 \quad \text{(A-9)}$$

$$D_2 = c_2 + f_2 - k_2 - l_2 - n_2 \quad \text{(A-10)}$$

$$E_2 = d_2 + e_2 + k_2 + l_2 + m_2 \quad \text{(A-11)}$$

$$F_2 = k_2 + i_2 \quad \text{(A-12)}$$

$$G_2 = l_2 - i_2 \quad \text{(A-13)}$$

$$H_2 = -k_2 + j_2 \quad \text{(A-14)}$$

$$I_2 = -l_2 - j_2 \quad \text{(A-15)}$$

$$J_2 = -\frac{\theta}{\Delta t} \quad \text{(A-16)}$$

(A-17)

$$a_2 = -\frac{\rho_0 g}{\Delta x^2}\left(\frac{(\frac{k_x}{\mu})^{n+1,m}_{i,j}.(\frac{k_x}{\mu})^{n+1,m}_{i-1,j}}{(\frac{k_x}{\mu})^{n+1,m}_{i,j}+(\frac{k_x}{\mu})^{n+1,m}_{i-1,j}}\right)\left(h_{f\,i,j}^{\,n+1,m+1} - h_{f\,i-1,j}^{\,n+1,m+1}\right)$$

$$b_2 = \frac{\rho_0 g}{\Delta x^2}\left(\frac{(\frac{k_x}{\mu})^{n+1,m}_{i,j}.(\frac{k_x}{\mu})^{n+1,m}_{i+1,j}}{(\frac{k_x}{\mu})^{n+1,m}_{i,j}+(\frac{k_x}{\mu})^{n+1,m}_{i+1,j}}\right)\left(h_{f\,i+1,j}^{\,n+1,m+1} - h_{f\,i,j}^{\,n+1,m+1}\right)$$

$$c_2 = -\frac{\rho_0 g}{\Delta z^2}\left(\frac{(\frac{k_z}{\mu})^{n+1,m}_{i,j}.(\frac{k_z}{\mu})^{n+1,m}_{i,j-1}}{(\frac{k_z}{\mu})^{n+1,m}_{i,j}+(\frac{k_z}{\mu})^{n+1,m}_{i,j-1}}\right)\left\{h_{f\,i,j}^{\,n+1,m+1} - h_{f\,i,j-1}^{\,n+1,m+1} + \Delta z\,.\left(\frac{(\frac{2\rho^{n+1,m}_{i,j}.\rho^{n+1,m}_{i,j-1}}{\rho^{n+1,m}_{i,j}+\rho^{n+1,m}_{i,j-1}})-\rho_0}{\rho_0}\right)\right\} \quad \text{(A-19)}$$

$$d_2 = \frac{\rho_0 g}{\Delta z^2}\left(\frac{(\frac{k_z}{\mu})^{n+1,m}_{i,j}.(\frac{k_z}{\mu})^{n+1,m}_{i,j+1}}{(\frac{k_z}{\mu})^{n+1,m}_{i,j}+(\frac{k_z}{\mu})^{n+1,m}_{i,j+1}}\right)\left\{h_{f\,i,j+1}^{\,n+1,m+1} - h_{f\,i,j}^{\,n+1,m+1} + \Delta z\,.\left(\frac{(\frac{2\rho^{n+1,m}_{i,j}.\rho^{n+1,m}_{i,j+1}}{\rho^{n+1,m}_{i,j}+\rho^{n+1,m}_{i,j+1}})-\rho_0}{\rho_0}\right)\right\} \quad \text{(A-20)}$$

$$g_2 = \frac{1}{\Delta x^2}\left(\frac{D_{xx\,i,j}^{\,n+1,m} + D_{xx\,i+1,j}^{\,n+1,m}}{2}\right) \quad \text{(A-21)}$$

$$h_2 = -\frac{1}{\Delta x^2}\left(\frac{D_{xx\,i,j}^{\,n+1,m} + D_{xx\,i-1,j}^{\,n+1,m}}{2}\right) \quad \text{(A-22)}$$

$$i_2 = \frac{1}{4\Delta x\Delta z}\left(\frac{D_{xz\,i,j}^{\,n+1,m} + D_{xz\,i,j+1}^{\,n+1,m}}{2}\right) \quad \text{(A-23)}$$

$$j_2 = -\frac{1}{4\Delta x\Delta z}\left(\frac{D_{xz\,i,j}^{\,n+1,m} + D_{xz\,i,j-1}^{\,n+1,m}}{2}\right) \quad \text{(A-24)}$$

$$k_2 = \frac{1}{4\Delta x\Delta z}\left(\frac{D_{xz\,i,j}^{\,n+1,m} + D_{xz\,i+1,j}^{\,n+1,m}}{2}\right) \quad \text{(A-25)}$$

$$l_2 = -\frac{1}{4\Delta x\Delta z}\left(\frac{D_{xz\,i,j}^{\,n+1,m} + D_{xz\,i-1,j}^{\,n+1,m}}{2}\right) \quad \text{(A-26)}$$

$$m_2 = \frac{1}{\Delta z^2}\left(\frac{D_{zz\,i,j}^{\,n+1,m} + D_{zz\,i,j+1}^{\,n+1,m}}{2}\right) \quad \text{(A-27)}$$

$$n_2 = -\frac{1}{\Delta z^2}\left(\frac{D_{zz\,i,j}^{\,n+1,m} + D_{zz\,i,j-1}^{\,n+1,m}}{2}\right) \quad \text{(A-28)}$$

$$o_2 = C^{\,n+1,m+1}_{i,j}(1-\theta)\xi\rho_0 g\left(\frac{h_{f\,i,j}^{\,n+1,m+1} - h_{f\,i,j}^{\,n,m+1}}{\Delta t}\right) \quad \text{(A-29)}$$

where ξ is soil compressibility.